Aerogeophysics and light detecting and ranging (LiDAR)-based lineament interpretation of Finland at the scale of 1:500 000

Jon Engström[1,2], Mira Markovaara-Koivisto[1], Nikolas Ovaskainen[1,3], Nicklas Nordbäck[1,3], Markku Paananen[1], Ismo Aaltonen[1,3], Annu Martinkauppi[1], Heidi Laxström[1], Henrik Wik[1]

[1]Geological Survey of Finland, P.O. Box 96, FI-02151, Espoo, Finland

[2]Åbo Akademi University, FI-20500, Turku, Finland

[3]University of Turku, FI-20500, Turku, Finland

Correspondence to: Jon Engström (jon.engstrom@gtk.fi)

Abstract. Lineaments, linear structures on the surface of the Earth, often represent the surface expressions of brittle structures, e.g., fault zones and fracture zones, or ductile shear zones. In addition, they may also represent other geological features such as lithological contacts, tectonic boundaries and Quaternary structures, or potentially a superposition of any of these. A lineament interpretation is usually the first step in the structural assessment of a crystalline bedrock setting, and the lineaments can further be used as basis for scientific research to more accurately determine the location of the previously mentioned various geological features. In this study, a multi-source lineament interpretation was performed within ArcGIS for the whole of Finland, based on light detecting and ranging (LiDAR), aerogeophysical and bathymetric raster data. The lineament database enhances the capability to produce more accurate geological maps for various geological purposes in Finland.

1 Introduction

Topographical highs and depressions, such as valleys and slopes, form sub-linear continuities on the surface of the Earth. Lineaments were first defined as lines interpreted, i.e., manually drawn by a geologist, along these topographical continuities (Hobbs, 1904, 1911). The accuracy of lineament interpretation continues to evolve and improve as new and better-quality datasets have become available for lineament interpretation. Notably, the introduction of aerial photos and later satellite images significantly improved the possible accuracy of lineament interpretation (Abrams et al., 1985; Tailor et al., 1986). Furthermore, when large-scale airborne geophysical measurement survey campaigns were initiated approximately fifty years ago, the resulting datasets could be used to complement the interpretation previously based almost solely on topography. Today, lineament interpretations are primarily based on photographic, topographical and geophysical source raster datasets (Tirén, 1991; Middleton et al., 2015; Yeomans et al., 2019; Ahmadi and Pekkan, 2021; Ceccato et al., 2022). These are, for example, aerial photos, elevation data, multi-spectral sensing, laser, radar and airborne geophysical data comprising magnetic and electromagnetic radiation measurements, and gravimetric measurements. Interpreting lineaments using these sources has uncertainties, which are both objective, i.e., related to the data and methods (see, e.g., Rohrbaugh et al., 2002; Zeeb et al., 2013) and subjective, i.e., related to the interpreter(s) (see, e.g., Bond et al., 2007; Scheiber et al., 2015). To increase the interpretation speed and to minimize subjective uncertainty, several semi-automatic and automatic interpretation methods have been developed in addition to the manual interpretation method (e.g., Middleton et al., 2015; Aghaee et al., 2021; Ahmadi and Pekkan, 2021), but even though these are rapid methods to interpret lineaments, the automatically produced datasets often need manual corrections and reviews before they can be used further (Ramli et al., 2010; Ahmadi and Pekkan, 2021). The first country-wide lineament interpretation in Finland was performed in the 1980s by the Geological Survey of Finland (GTK) (Vuorela and Äikäs, 1984), when the screening for a suitable nuclear waste disposal site commenced. An updated interpretation was performed 20 years ago (Kuivamäki, 2000).

During recent years, a higher demand for groundwater, geothermal solutions, and increased use of underground rock volumes in construction projects has led to higher requirements for the understanding of subsurface brittle bedrock structures, e.g., fractures and faults (Ledésert et al., 1993; Berkowitz, 2002; Geiger and Emmanuel, 2010; Ceccato et al., 2022). Consequently, this has resulted in the need for a new and improved lineament interpretation for identifying brittle structures reaching the surface. Another motivation for an updated and new lineament interpretation was initiated by the release of the new high-resolution light detection and ranging (LiDAR) data from the National Land Survey of Finland (0.5 points per square metre). Using these new data, an updated Digital Elevation Model (DEM) could be compiled for the entirety of Finland. As the DEM is the primary dataset used previously for lineament interpretation, the higher

resolution (2 m grid cell size) enables much higher accuracy in the interpretation of lineaments. Because of the very high level of detail of the new DEM, the resolution of the model is no longer the major limiting factor in interpretation, but rather the time investment required for the interpretation.

Our new country-wide lineament interpretation, performed at a single scale of observation with the representative fraction of 1:500 000, started in 2019 and was finished in 2021. Our approach was to produce three separate lineament datasets (topographic, magnetic and electromagnetic), and to then integrate them into a single integrated lineament dataset in which lineaments from the separate source datasets are combined. The present work provides a new lineament database for Finland, which is more flexible for statistical analysis than prior interpretations and contains unique identifiers, along with crucial metadata for each interpreted lineament, to enable consistent references to the data and to allow tracking of the source of each lineament. However, the lineaments interpreted in this study can be assumed to represent several different geological features, such as ductile shear zones, lithological contacts, dykes and brittle structures (e.g., faults and fractures). These features have primarily been formed by tectonic processes, but, in addition, glacial processes can also produce linear structures that can be observed as lineaments, such as end moraine ridges and eskers (Henderson, 1988; Krabbendam and Bradwell, 2014; Skyttä et al., 2015). Despite the broad variation of lineament-forming processes and the associated uncertainties of individual lineaments and their geological origin, the lineament database can be used further for various geological applications, such as for tunnel and groundwater projects, geothermal site studies and mineral exploration. The database can, for example, be used as an aid in regional geological tectonic studies (Gabrielsen et al., 2002; Engström and Klint, 2014), or applied as a basis for more detailed site characterization studies (Kuivamäki, 2000; Munier, 2004; Korhonen et al., 2005; DesRoches et al., 2018). As part of this study, an initial lineament field examination was performed at selected locations for two lineaments in southern Finland.

2 Materials and methods

The multiscale lineament datasets were mapped in ArcGIS (© ESRI) using remote sensing methods based on airborne topographic LiDAR data (Abdullah et al., 2013; Soliman and Han, 2019) integrated with bathymetric and aerogeophysical raster datasets (Figure 1). The interpretation scale was set to 1:500 000, which roughly represents 300 m cell size raster images. The workflow for the lineament determination included initial compilation of three separate datasets, consisting of total magnetic (Mag) (see section 2.1), electromagnetic (EM) (see section 2.2) and LiDAR, together with bathymetry (see section 2.3) (Figure 1). All vector data were validated according to the procedures described in section 2.4 and afterwards integrated in concurrence with the steps described in section 2.5. Ideally, to better understand the geological nature of each lineament, the lineaments should be examined via fieldwork or drilling after the validation step.
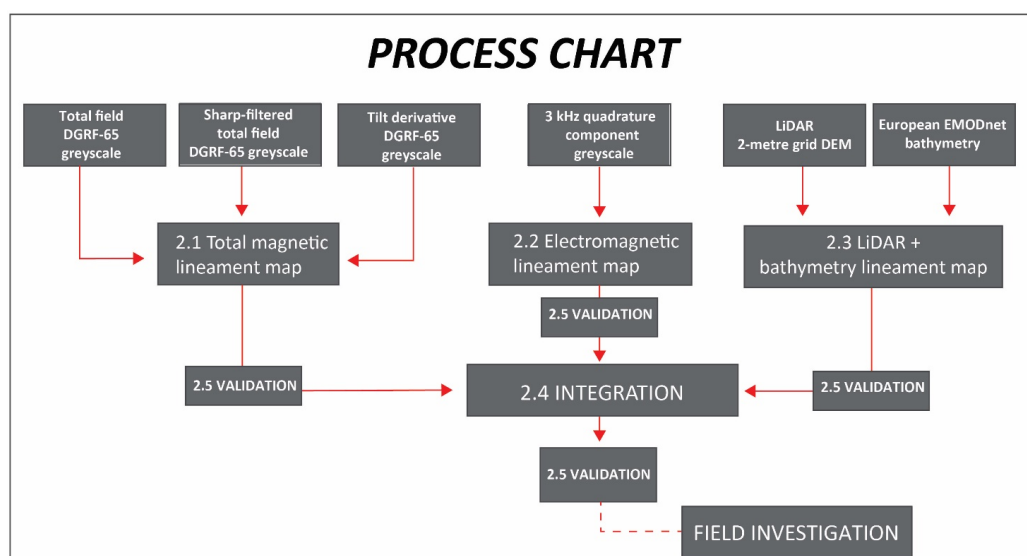
Figure 1: The lineament interpretation process chart illustrating all relevant steps for the interpretation and the source data used in the interpretation.

2.1 Total magnetic (Mag)

The total magnetic lineaments were interpreted from the aerogeophysical data mapped by GTK as part of national low-altitude airborne surveying projects between 1972–2004 (Hautaniemi et al., 2005). In the aerogeophysical measurement campaign, magnetic measurements were taken from an altitude of 30 m and with a line spacing of 200 m. The measurements were compiled into several types of magnetic rasters with a cell size of 50 m. For lineament interpretation, we selected three different magnetic rasters consisting of total field DGRF-65 greyscale, sharp-filtered total field DGRF-65 greyscale and tilt derivative DGRF-65 greyscale (Verduzco et al., 2004) (Figure 1; Appendix A-C). Magnetic lineaments were interpreted from these maps based on both magnetic maxima and minima. The geophysical basis for the lineaments appearing as maxima compared to the surrounding rock is that oxidizing fluids intruding the rock during metamorphism may have deposited magnetic minerals, such as magnetite and pyrrhotite, into fractures or as pervasive dissemination. On the other hand, the magnetitic minima may have formed when reducing metamorphic fluids decomposed the magnetitic minerals. Low-temperature rock weathering may also physically and chemically decompose magnetitic minerals, consequently causing a local magnetitic minimum. In these cases, magnetite is oxidized into haematite and pyrrhotite into goethite and elemental sulphur. In addition to magnetic maxima and minima, lineaments were also interpreted at breaks in the magnetic texture, where faults have caused discontinuities in the bedrock (Paananen, 2013; Middleton et al., 2015).

2.2 Electromagnetic (EM)

The electromagnetic lineaments were interpreted from aerogeophysical frequency domain data collected during the same national survey campaign between 1972–2004 (Hautaniemi et al., 2005). The electromagnetic data were visualized using the 3 kHz quadrature component greyscale (Figure 1; Appendix D). In the interpretation process, only the quadrature component was considered, because it is more sensitive to poor conductors and not affected by magnetic properties, in contrast to the in-phase component. Lineaments are interpreted at the locations indicating resistivity minima. The geophysical basis for using resistivity minima is that the rock material in brittle deformation zones contains groundwater and the fractures may be coated with conducting minerals, such as graphite, sulphides and clay minerals. In addition, the brittle deformation zones form valleys, which are filled with conductive sediments and soil material such as peat. Furthermore, as these structures represent topographic depressions, they also act as collectors of rain and seepage water (Paananen, 2013; Middleton et al., 2015). Larger water bodies cause electromagnetic anomalies indicating decreased resistivity.

2.3 LiDAR DEM and bathymetry (~~LiDAR~~)

The primary dataset used in the interpretation was the highly accurate low-altitude airborne LiDAR-based topographical digital elevation model (DEM). To produce the DEM, the high-resolution LiDAR point cloud database, collected by the National Land Survey of Finland, was processed at GTK into a DEM that represents the bare earth surface. The point density for the cloud point data is 0.5 points per square metre and the elevation accuracy is 0.3 m. The process at GTK started by querying the point cloud database for only those points representing the surface of the Earth that were already classified by the National Land Survey of Finland. The points were then triangulated to form a terrain surface mesh and subsequently interpolated with the natural neighbour algorithm into a 2 m grid size DEM raster. We used the visualization described by Palmu et al. (2015), with the height colour classification set to calculate statistics from the current extent of the display. To highlight lineaments, we used multidirectional oblique-weighted hillshade (Jennes, 2013) without vertical exaggeration. Transparency was set at 50% for the hillshade layer placed on top of the DEM. To identify and extend lineaments into the sea areas, we used the sea-bottom topography, referred to as bathymetry, acquired from the European EMODnet Bathymetry Consortium (2018) open-source bathymetric data, retrieved from the website in March 2019 (Figure 1; Appendix E). The EMODnet bathymetry dataset is an elevation model for the seabed with a cell size of circa 115 m.

2.4 Integration

Integration of the separate lineament vector data was performed by merging electromagnetic, magnetic and LiDAR lineaments into one ESRI database layer with all lineaments superimposed. Overlapping lineaments were then removed in the following order: 1) electromagnetic lineaments overlapping magnetic or LiDAR lineaments and 2) magnetic lineaments overlapping LiDAR lineaments. In case the ends of the lineaments to be removed were branched off from the remaining lineament, the branches were preserved, and only the overlapping part was removed. Because the measurement point density and the resolution of the produced LiDAR raster DEM was the highest of all the source dataset rasters, the

130 LiDAR lineaments were used as a basis for the integration. Magnetic maps were considered more informative than the electromagnetic map due to having several different magnetic map layers. As part of the integration step, information on which layers the lineament had been observed in was stored in the attribute fields for data source classes and reliability. If the different lineaments overlapped with another lineament, even partly, this information was documented, and the lineaments were integrated. The reliability of an integrated lineament is considered to be higher if the lineament has been
135 interpreted from more than one source (DesRoches et al., 2018).

2.5 Metadata and validation

The lineament vector data interpreted from the four raster sources consisted of geometric polylines. We supplemented the geometric information with a defined set of attribute metadata indicating, for example, the source raster and digitizer of each lineament (Table 1). Furthermore, the topological relationship (Manzocchi, 2002; Sanderson and Nixon, 2015)
140 between the traces was preserved using the snapping functionality in ArcGIS. However, to keep the geometries, various metadata and the topological relations consistent between multiple interpreters and raster sources, a validation method was employed for all vector datasets. For this purpose, we first used the trace validation functionality of fractopo, a Python library (Ovaskainen et al., 2022a), to validate the geometry of individual traces and to validate the abutment relationships between the traces. Furthermore, we used the pandera Python library (Bantilan, 2020) to validate the associated metadata
145 fields in the lineament datasets by defining strict rules (Table 1) for each field. The code for combining fractopo trace validation and pandera metadata validation capabilities is freely available on Zenodo and GitHub (Ovaskainen, 2022).

Table 1: Metadata for the various lineament datasets.

Column	Description	Validation rules	Example
Lineament_ID	A unique identifier for each lineament.	The prefix depends on the data source and scale. The full identifier must be unique within its own dataset.	LiDAR_10
Data_Source	Interpretation source.	Consists of 'EM', 'Mag' and 'LiDAR' identifiers separated by a plus symbol.	LiDAR+EM
Certainty	Identifies whether only LiDAR or LiDAR and geophysical sources have been used.	Either '1_Geoph_OR_LiDAR' or '2_Geoph_AND_LiDAR'.	2_Geoph_AND_LiDAR
Scale	Scale at which interpretation has been performed.	Consists of pre-defined scales such as 1:500 000.	1:500 000
Operator	Interpreter of the lineament.	One of set interpreters.	Engström J.
Date	Date of digitization.	A valid datetime string.	2019-04-11
Remarks	A free-form text field for miscellaneous information related to the lineament.	-	Potential end moraine related to Salpausselkä II.

The employed geometric and topological validation enables seamless usage of the lineament datasets in geospatial fracture
150 network analyses of, for example, orientation or connectivity (Sanderson and Nixon, 2015; Ovaskainen et al., 2022a). All traces must be geometrically continuous without any gaps in the geometry and sublinear without abrupt sharp turns. We allowed two types of interactions between lineament traces: A trace can abut another trace, defining a Y-node interaction, or crosscut another trace, resulting in an X-node interaction between the traces (Manzocchi, 2002). To define a valid abutment interaction between two traces, we used the distance value of the trace endpoint to the closest point along the
155 other trace. If this distance value was below our set threshold value of 0.001 m, we classified the first trace as abutting

the other trace. To avoid all inconsistent arrangements of trace interactions, fractopo has a set number of validation errors that it finds and highlights (Figure 2). Using this highlighting, we methodically removed all inconsistent trace interactions, such as V-nodes (Sanderson and Nixon, 2015). We validated all four separate lineament vector datasets using the above procedure.
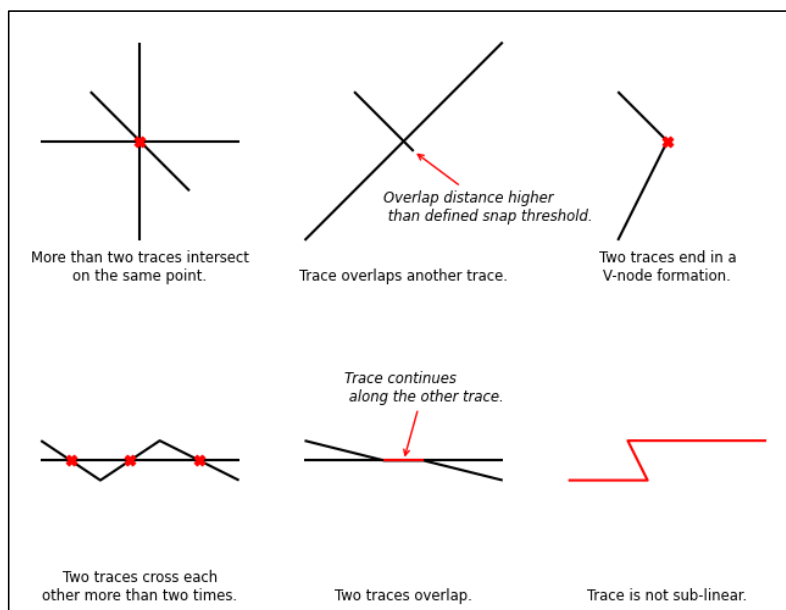
Figure 2: A subset of the topological arrangements that are identified as errors by fractopo. See fractopo documentation (https://fractopo.readthedocs.io/en/latest/validation/errors.html) for a full listing.

The subjective uncertainty concerning interpretation biases for various operators can be reduced with a proper interpretation scheme and by setting a fixed scale for the interpretation (Scheiber et al., 2015). Therefore, an internal
165   workshop between operators was organised before the work commenced. Objective uncertainties that are related to the data and methods of interpretation may, for example, be associated with the nature and extent of coverage with overburden that masks the bedrock surface. As we attempted to create continuous lineaments, it was unavoidable that some parts of lineaments might not be visible in any of the source rasters. In these cases, the lineaments were often continued across masked terrain, and the extent of interpolation in these cases was subject to operator bias. Furthermore, as the
170   representation of the lineaments in each unique source raster differs, consequent subjective uncertainty manifests both during interpretation and in the integration phase, where the diverse lineaments are combined. In addition, objective uncertainty associated with a poor magnetic contrast between the rock mass and potential fractured zones can also limit the interpretation of lineaments from airborne magnetic survey data (Scheiber et al., 2015; DesRoches et al., 2018). Due to these and the numerous other uncertainties in lineament interpretation, verification of the interpreted lineaments is
175   always preferable, but since lineament verification is a rigorous and time-consuming task, it is almost impossible to verify all or even a part of the lineaments and determine their geological characteristics in the field. Field mapping can typically only be conducted in quarries or road cuts, where detailed structural observations are possible. Usually, the centre of the lineament (core of the fault zone) is masked by Quaternary deposits, while the outer parts of the lineament (damage zone of the fault zone) can be visible. To exemplify the process of the field investigation of interpreted lineaments, two
180   lineaments were examined in this study at selected locations, at a roadcut and a quarry that intersected these lineaments, to survey their local geological characteristics.

2.6   Analysis

Here, we present first-pass lineament orientation and topological analysis results from lineaments from each raster source, along with results from the integrated lineaments. Specifically, we present equal-area length-weighted rose plots
185   (Sanderson and Peacock, 2020) to visualize the orientations of lineaments for each raster source and ternary node, and branch proportion plots to visualize differences in topological connectivity between the different lineament datasets

(Manzocchi, 2002; Sanderson and Nixon, 2015). As the lineament interpretation covers the entirety of Finland, the lithology and tectonic setting varies significantly within the interpretation area, which probably affects the characteristics of the lineaments of different areas. To analyse this variation, we also separately present orientation analysis results for the integrated lineaments of each tectonic province (Nironen, 2017).

3   Results

The three (magnetic, electromagnetic and LiDAR) lineament vector datasets were interpreted independently from each other, and the results from these are presented below. Several operators, i.e., geologists or geophysicists working at GTK, participated in the interpretation. To minimize the subjective bias of the different operators, a similar operation scheme was used. The interpretations were gathered into lineament vector datasets that were categorized according to the source raster used. These can be used independently from each other. The integrated vector dataset was produced as the final product in the lineament database. A statistical overview of the lineament vector datasets, based on number and length, is gathered in Table 2.

Table 2: Statistical data for the magnetic, electromagnetic, LiDAR and integrated lineaments.

Magnetic Lineaments						
Minimum (m)	Lower quartile (m)	Median (m)	Mean (m)	Upper quartile (m)	Maximum (m)	Number
3947	15 182	23 023	28 908	36 376	146 314	983
Electromagnetic Lineaments						
Minimum (m)	Lower quartile (m)	Median (m)	Mean (m)	Upper quartile (m)	Maximum (m)	Number
3700	14 457	22 517	29 181	35 600	300 528	1244
LiDAR and Bathymetric Lineaments						
Minimum (m)	Lower quartile (m)	Median (m)	Mean (m)	Upper quartile (m)	Maximum (m)	Number
2580	15 358	24 119	31 688	38 295	298 717	1579
Integrated Lineaments						
Minimum (m)	Lower quartile (m)	Median (m)	Mean (m)	Upper quartile (m)	Maximum (m)	Number
2566	13 425	21 562	27 290	33 845	305 059	3476

3.1   Magnetic

The 983 magnetic lineaments were evenly scattered within the whole country, but with fewer lineaments within the Rapakivi batholite in the southeastern part of Finland (Figure 3). Magnetic maps continue partly offshore, enabling the interpretation of lineaments at sea. The lineament lengths varied from 3.9 km to 146.3 km, while the median length was 23 km (Table 2).
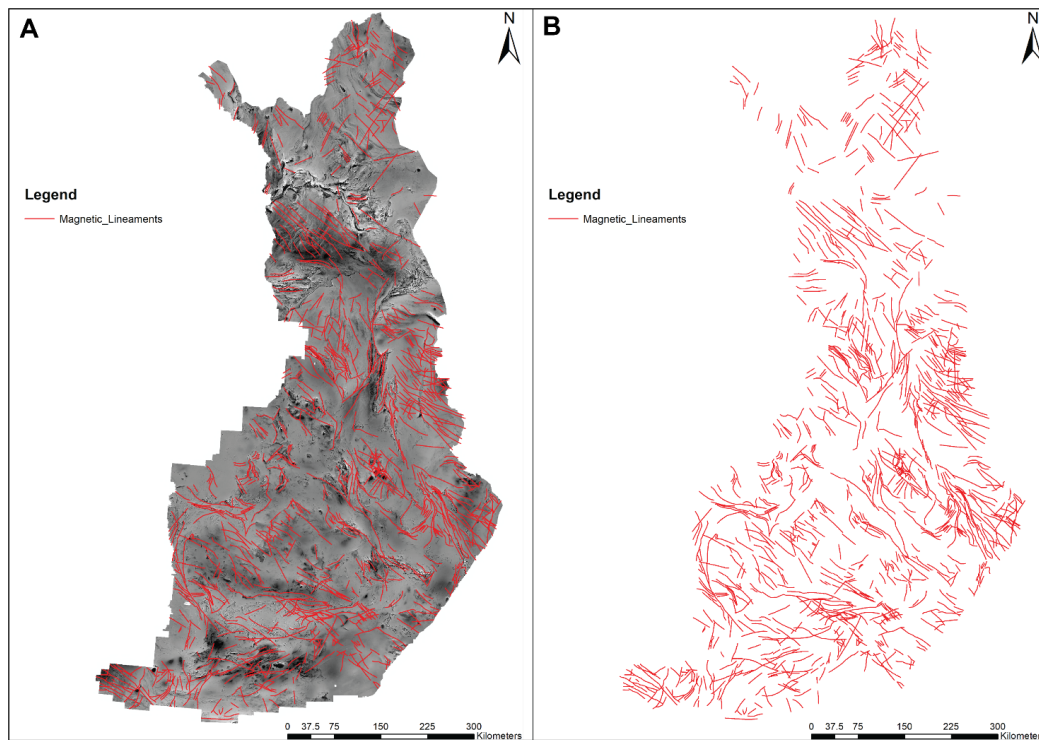
Figure 3: A) Magnetic lineaments from the interpretation area of Finland, with the total magnetic base map (Geological Survey of Finland, 2007a) in the background. B) Magnetic lineaments from the interpretation area of Finland.

3.2 Electromagnetic

210   The 1244 electromagnetic lineaments were consistently distributed throughout the country (Figure 4). However, within the Rapakivi batholite in southeast Finland, the lineaments were even more scarce than in the magnetic rasters, and only a few linear anomalies were thus interpreted. Bodies of water have low electrical resistivity and they therefore appear as electromagnetic minima in the data. In sea areas, the electromagnetic lineaments are interpreted between or next to the areas of higher resistivity. The lineament lengths varied from 3.7 km to 300.5 km, while the median length was 22.5 km
215   (Table 2).
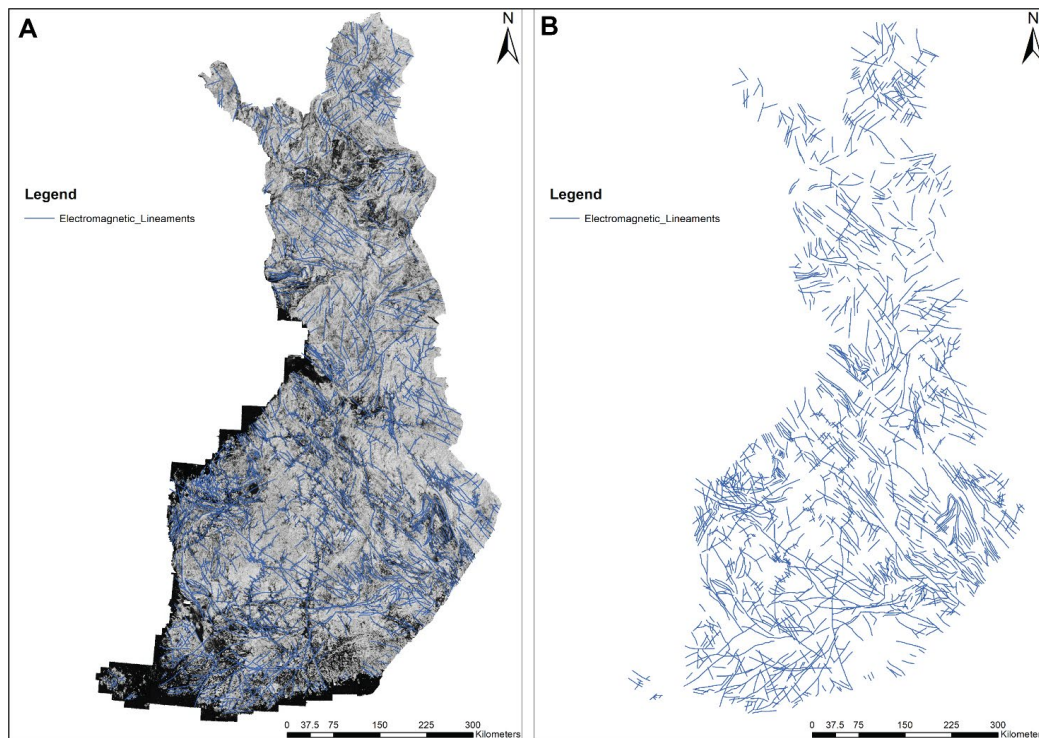
Figure 4: A) Electromagnetic lineaments from the interpretation area of Finland, with the electromagnetic base map (Geological Survey of Finland, 2007b) in the background. B) Electromagnetic lineaments from the interpretation area of Finland.

3.3   LiDAR and bathymetry

Overall, 1579 topographical lineaments were interpreted within the whole country, including LiDAR-based terrestrial and the sea-bottom bathymetry-based lineaments (Figure 5). The lineaments were evenly scattered, except in the western part of Finland, in Ostrobothnia, where a thick overburden of Quaternary deposits partially masks the underlying topography, thus hindering interpretation in this area. The LiDAR and bathymetric dataset is the most extensive one, covering both terrestrial and sea areas. The lineament lengths varied from 2.6 km to 298.7 km, while the median length was 24.1 km (Table 2).
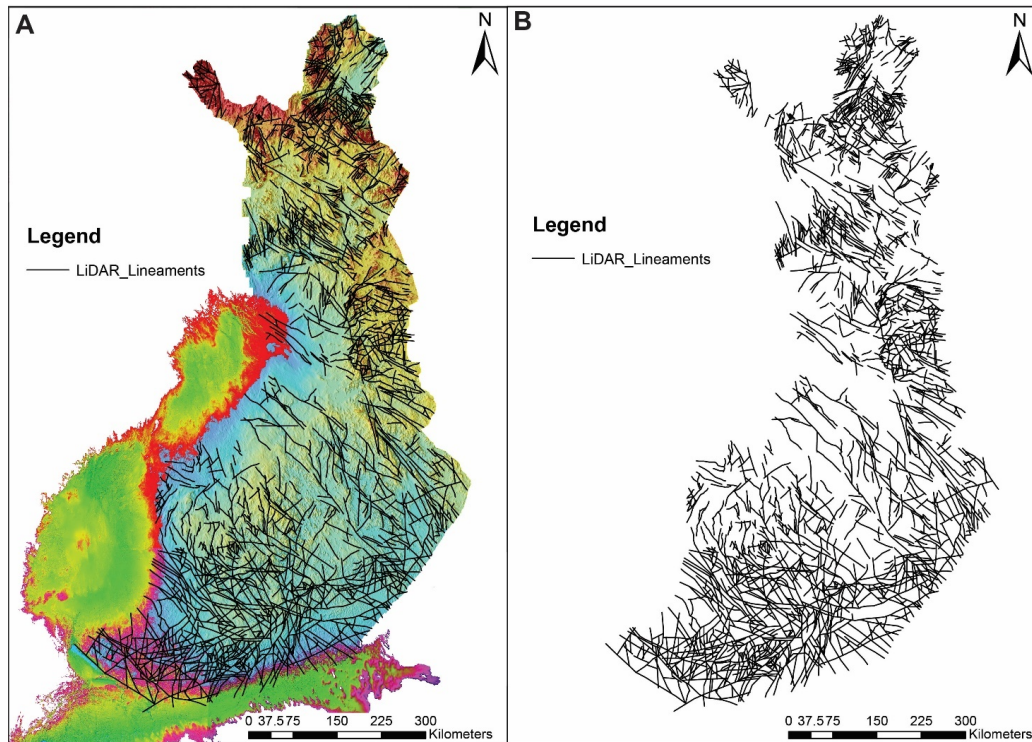
Figure 5: A) LiDAR and bathymetric lineaments from the interpretation area of Finland, with the topographic DEM in the background. Topographic DEM adapted from National Land Survey of Finland (2019) and European EMODnet Bathymetry Consortium (2018). B) LiDAR and bathymetric lineaments from the interpretation area of Finland.

3.4 Integration

The total number of magnetic, electromagnetic and LiDAR lineaments was 3806 (Figure 6A). After integration, 3476 lineaments remained in the integrated dataset (Figure 6B). The integrated lineaments were evenly scattered across the country. Their length varied from 2.6 km to 305.1 km, while the median length was 21.6 km (Table 2). The LiDAR lineaments were used as a basis for the integrated lineament interpretation, and were thus extended or modified based on the geophysical anomalies. An example of the integration process from southwest Finland is illustrated in Figure 7. The LiDAR lineaments were mainly modified in the integration, while the geophysical lineaments either remained in their entity or as small branches that diverged out from the larger LiDAR lineaments (Figure 7D).
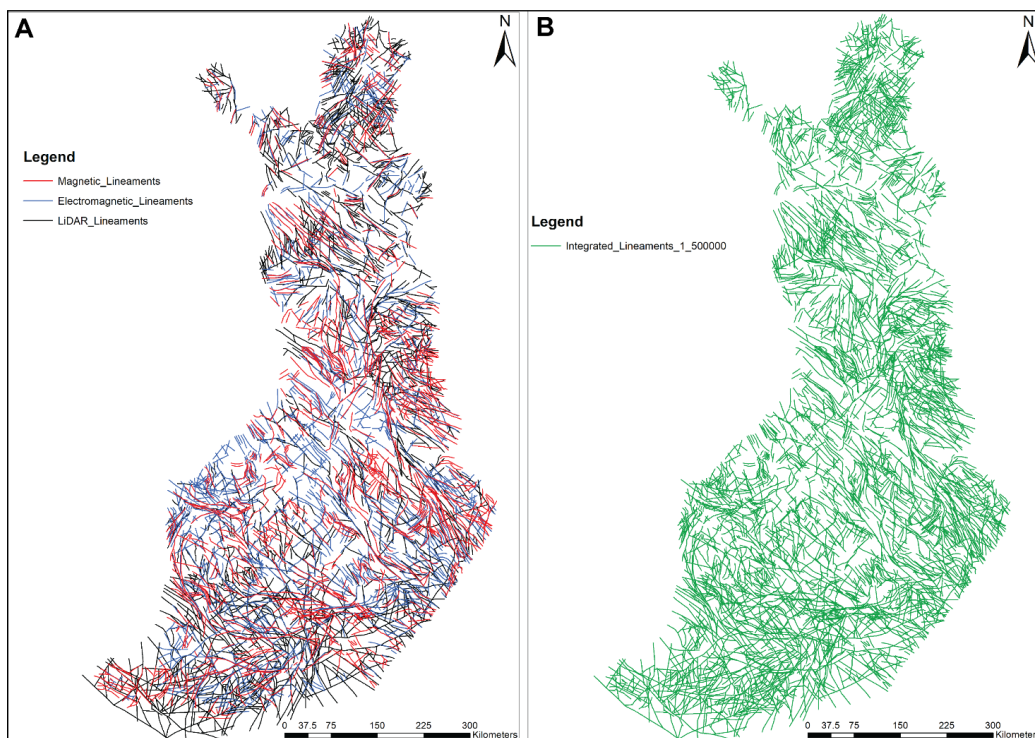
Figure 6: A) All interpreted lineaments defined by different colours from the interpretation area of Finland. B) The final integrated lineament interpretation.
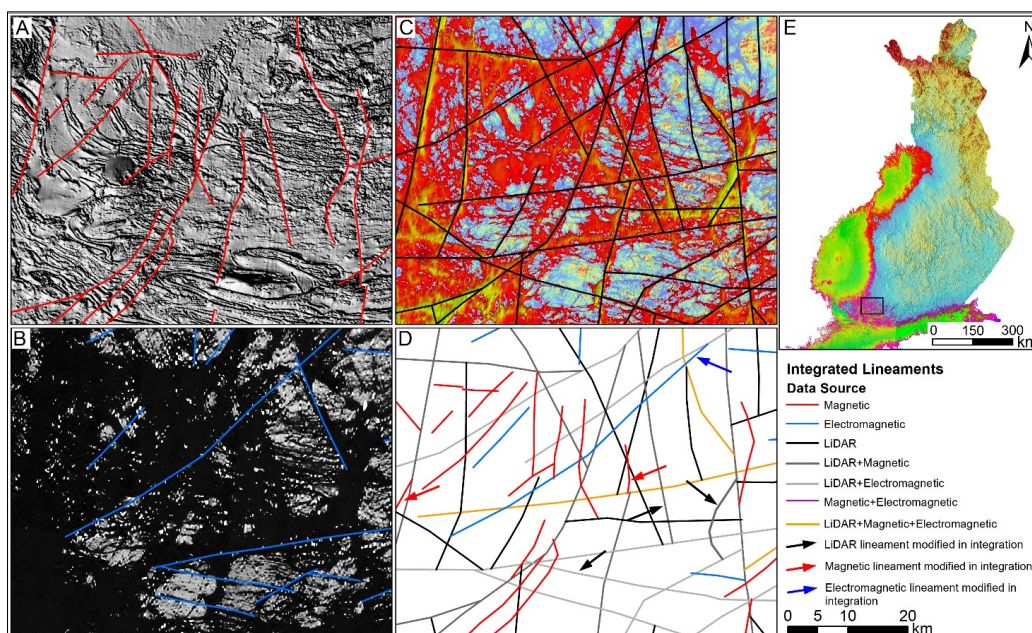
Figure 7: Integrated lineaments from southwest Finland. A) Magnetic lineaments with filtered magnetic greyscale as a raster map (Geological Survey of Finland, 2007a)). B) Electromagnetic lineaments with quadrature component greyscale as a raster map (Geological Survey of Finland, 2007b). C) LiDAR lineaments with LiDAR and bathymetry as a raster map. Topographic DEM adapted from National Land Survey of Finland (2019) and European EMODnet Bathymetry Consortium (2018). D) Black arrows indicate the 250 locations of LiDAR lineament modifications performed during integration, red arrows indicate magnetic lineaments and blue arrows indicate electromagnetic lineaments. E) LiDAR and bathymetric raster map of Finland. Topographic DEM adapted from National Land Survey of Finland (2019) and European EMODnet Bathymetry Consortium (2018). The black box indicates the area of the lineaments in maps A–D.

255 Most of the integrated lineaments (2732 out of 3476) were interpreted from only one data source. The other 744 lineaments were fully or partly visible in at least two out of the LiDAR, electromagnetic and magnetic data sources. In total, 159 lineaments were fully or partly observed in all three data sources (Table 3).

Table 3: Trace length statistics for lineaments determined in different data sources; data compiled from the integrated dataset.

Data_Source	Minimum (m)	Lower Quartile (m)	Median (m)	Mean (m)	Upper Quartile (m)	Maximum (m)	Number
Mag	3562	12 834	19 094	22 963	28 492	109 282	697
EM	2566	10 889	17 676	21 093	27 223	97 769	985
LiDAR	2580	13 036	20 598	25 151	31 866	171 259	1050
LiDAR+EM	6936	23 908	35 199	44 143	52 941	305 059	282
LiDAR+Mag	7029	21 449	29 324	38 785	46 209	230 622	88
LiDAR+Mag+EM	14 054	28 873	44 062	53 823	66 670	176 697	159
Mag+EM	3702	17 873	28 301	33 722	44 863	106 795	215
Total							**3476**

3.5   Orientation and topological analysis of lineaments

260 All the rose plots (Figure 8) of lineaments from different sources, including the integrated lineaments, show distinct orientation maxima along a NW–SE-oriented axis. Besides this trend, the lineament orientations are quite scattered, without other defined orientation trend maxima, except for a weak NE–SW trend visible in the electromagnetic (EM) lineament rose plot. Overall, no distinct differences between the LiDAR, electromagnetic and magnetic lineament orientations are visible.
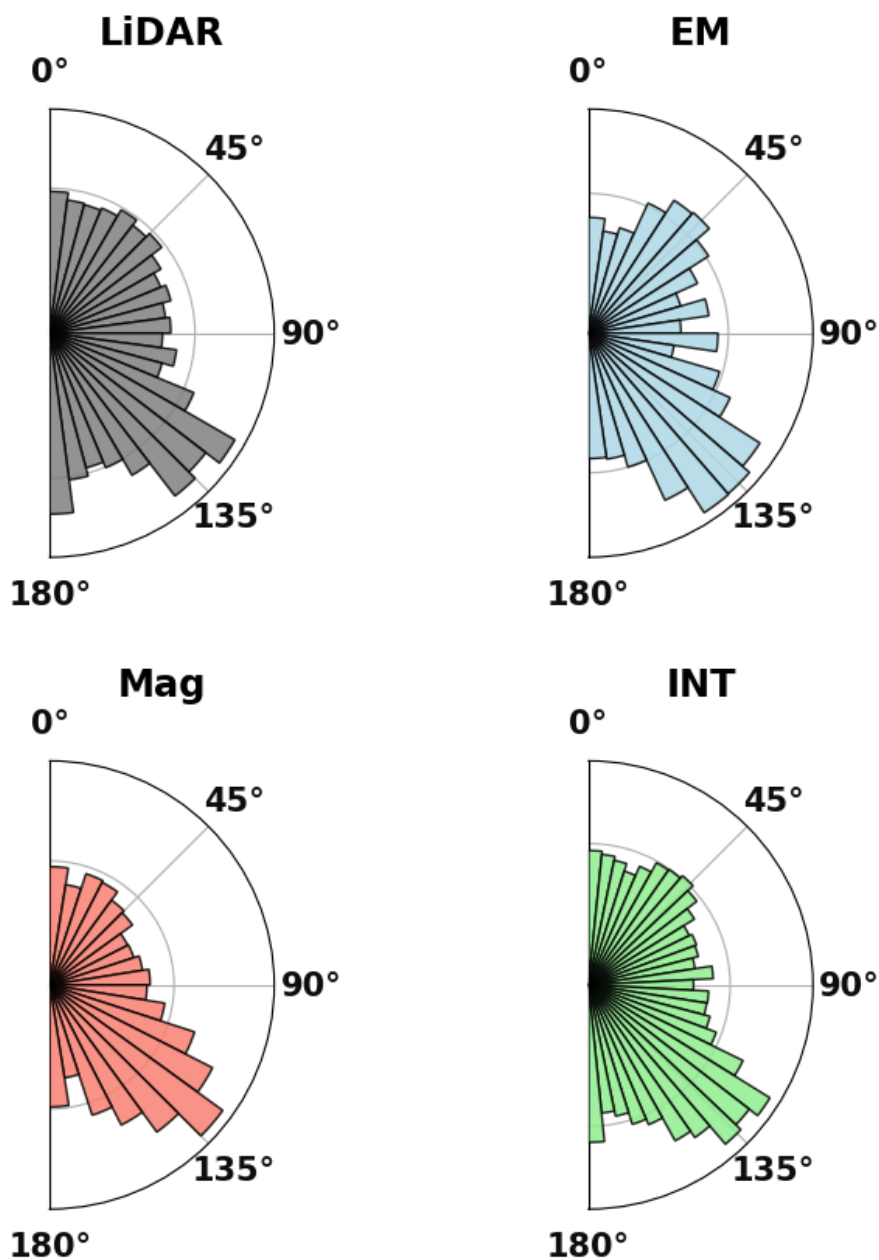
Figure 8: Rose plots the orientation of the lineaments from each raster source.

According to the ternary plots of node and branch proportions (Figure 9), the lineaments interpreted from aerogeophysical sources are less connected and have a significantly higher proportion of I-nodes (lineament ending in isolation). The magnetic lineaments also have a higher proportion of I-nodes compared to the electromagnetic lineaments. The integrated lineaments have similar node and branch proportions to the LiDAR lineaments, although with a distinctly higher number of X-nodes (Figure 9A).
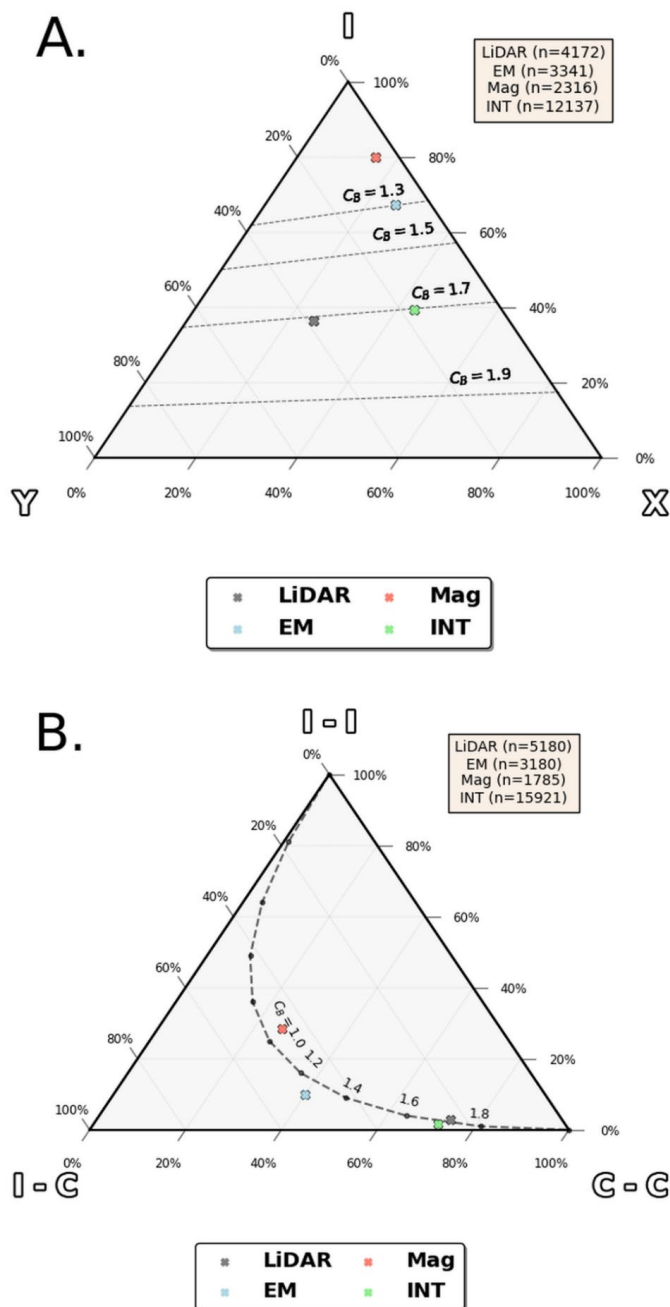
Figure 9: A) Ternary plot of topological nodes (X, Y and I). B) Ternary plot of topological branches (C-C, C-I and I-I). For both subfigures, the counts of nodes and branches, respectively, are indicated.

Subdivision of the integrated lineaments into the tectonic provinces of Finland and subsequent orientation analysis (Figure 10) does not highlight major differences between the orientations of lineaments from different tectonic provinces. The previously determined NW–SE trend is still visible in lineaments from most provinces, except for the Norrbotten province. However, the small areal extent and asymmetric shape of the Norrbotten province might cause a higher sampling bias compared to the other provinces. Similarly, the Central Karelia Subprovince has a limited sample count (n = 45), which should be kept in mind when making any further interpretations.
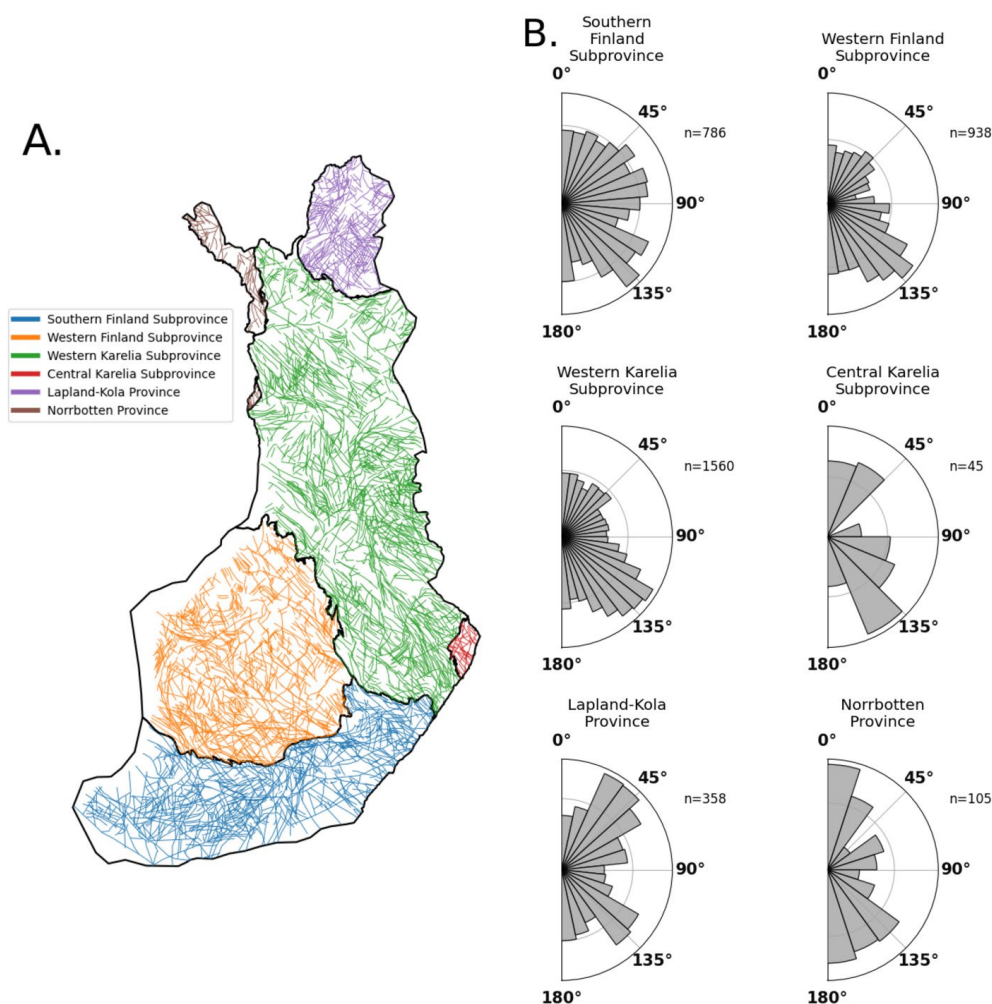
Figure 10: A) Integrated lineaments clipped to the boundaries of tectonic provinces by (Nironen, 2017), which are delineated by the black border polylines. B) Rose plots of the integrated lineaments, cropped to each tectonic province.

3.6 Field investigation of lineaments

During this study, two lineaments in southern Finland ("Lineament_ID" identifiers: INT_296 and INT_357) were examined in more detail to verify their geological nature at selected locations (Figure 11A). An E–W-oriented lineament (INT_296) located between Turku and Helsinki was examined in the near vicinity of Karkkila. The lineament was assumed to be the Somero–Karkkila Fault Zone (SKFZ) (Torvela and Kurhila, 2022), even though the core zone was not located in outcrops and only some brittle shear structures within the damage zone were available for mapping (Figure 11B). The shear structures within the damage zone were mapped as either parallel to the lineament or oriented NE–SW, but both sets of structures showed dip-slip kinematics on the slip surface, even though the slip orientation could not be

determined (Figure 11C&D). Since the core zone of the assumed fault zone could not be found, the overall kinematics of
295   the fault zone remained uncertain. Another NW–SE-oriented lineament (INT_357) that was investigated as part of this
study is related to a large ductile shear zone defined as the Kynsikangas Shear Zone (KSZ) (Reimers et al., 2018), located
north of Turku in the Kokemäki area (Figure 11A). The ductile KSZ is approximately 2 km wide (Figure 11G), and the
core of the shear zone is highly sheared and deformed. The core of the KSZ displays ductile stretching lineation with
sinistral kinematics (Figure 11E&F) (Reimers et al., 2018). Since the KSZ is a wide and prominent ductile shear zone,
300   the observed outcrops only represent a small portion of this structure (Figure 11G).
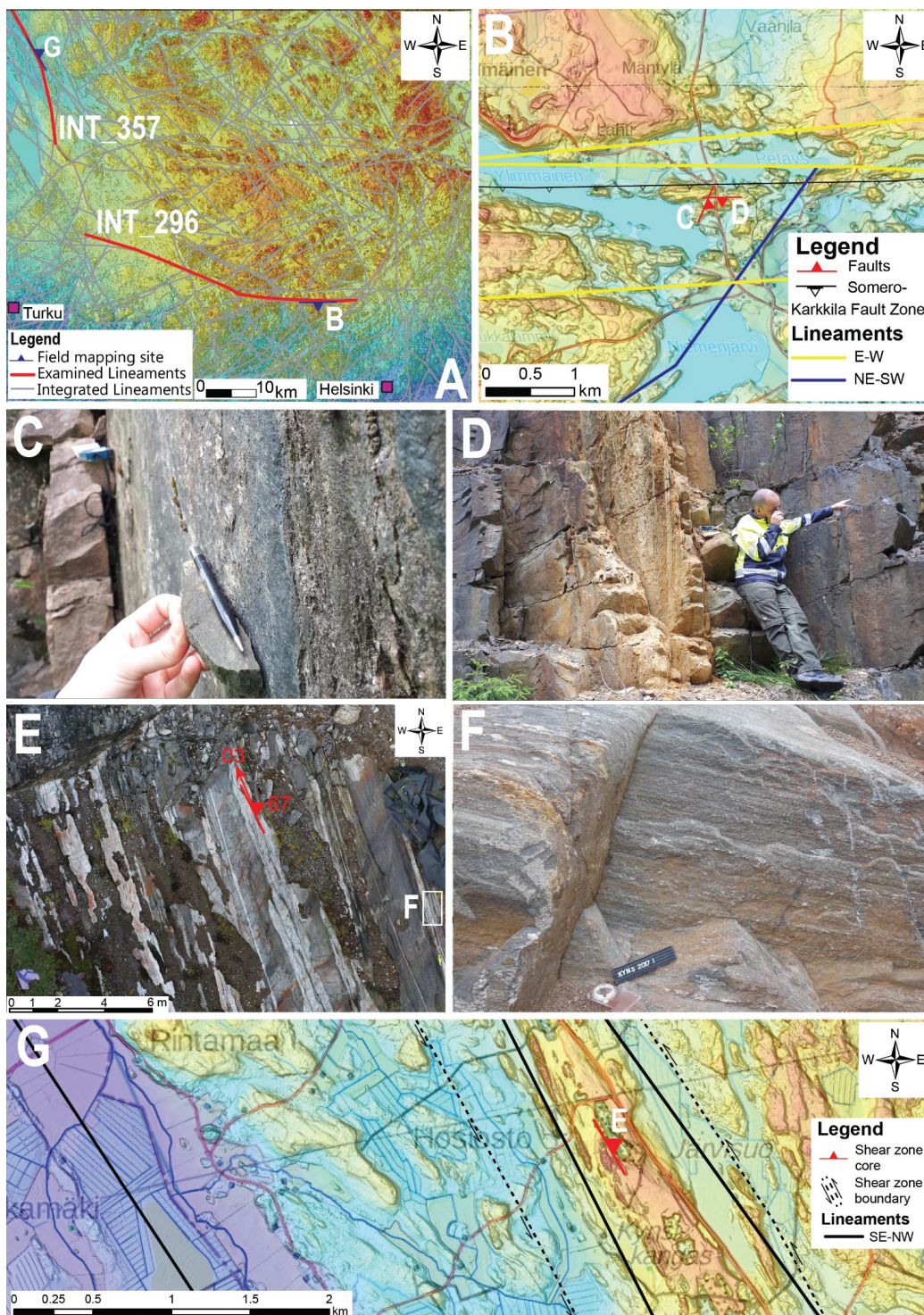
Figure 11: A) Integrated lineaments from southern Finland, with field investigated lineaments in red. LiDAR DEM adapted from National Land Survey of Finland (2019). B) The examination site for the E–W-oriented Somero–Karkkila Fault Zone (SKFZ). LiDAR DEM adapted from National Land Survey of Finland (2019). C) Photo of an NE–SW-oriented fault within the damage zone of the SKFZ. D) Photo of an E–W-oriented fault parallel to the SKFZ. E) Drone orthophoto of the core of a major ductile shear zone, the Kynsikangas Shear Zone (KSZ). F) Close-up photo of the KSZ, with prominent L-tectonites. G) Investigation site for the SE–NW-oriented lineament, the KSZ. LiDAR DEM adapted from National Land Survey of Finland (2019).

4   Discussion

This lineament study and the subsequent analysis differs in several respects from those previously performed in Finland and other countries. The most significant addition to the previous studies is the use of high-resolution LiDAR data. The final product, the integrated lineament vector dataset, represents a combined analysis of the electromagnetic, magnetic and topographical lineaments. Compared to the previous nationwide lineament studies (Vuorela and Äikäs, 1984; Kuivamäki, 2000), this current study used more accurate data sources (LiDAR DEM with a 2 m cell size, combined with bathymetric data) and involved more systematic documentation of lineament metadata. Globally, nationwide lineament surveys are scarce, and compared, for example, to the study performed by Gabrielsen et al. (2002) in Norway, our multi-source approach adds a higher level of confidence to the interpretation, as lineaments were identified from multiple raster datasets. DesRoches et al. (2018) also concluded in their study on a crystalline bedrock setting in Canada that a multi-source approach to lineament interpretation enhances the reliability of the interpretation. Our interpretation differs methodologically from past interpretations. For example, in comparison to the interpretation by Kuivamäki (2000), we did not allow circular lineaments. Furthermore, in contrast to the lineament interpretation of Korhonen et al. (2005), we applied a specific scale of observation in which all raster data sources were used with the same representative fraction of 1:500 000. Therefore, we avoided problems related to the lineament integration phase due, for instance, to differences in accuracy between source raster data, as described by Korhonen et al. (2005). Despite recent advances in automatic lineament interpretation methods (Middleton et al., 2015; Yeomans et al., 2019; Aghaee et al., 2021; Ahmadi and Pekkan, 2021), we opted for a manual interpretation approach due to the current limitations of automatic methods. The manual method has the advantage that the operator can learn to distinguish geological lineaments from non-geological features such as roads, railway lines, power-cables, canals and crop–field boundaries (Ramli et al., 2010), which in automatic interpretations requires a review. Automated methods developed for fracture trace detection are also limited in recognizing abutments and the topological relationship between lineaments (Prabhakaran et al., 2019).

We used strict geometric, topological and metadata validation methods to produce a cohesive vector dataset that is readily available for further analysis and also minimizes trace geometries and interactions that probably do not represent bedrock structures. The importance of the topological relationship between brittle structures and permeability, and subsequent fluid flow, has been highlighted in several studies on faults and fractures (Skyttä et al., 2021; Ceccato et al., 2022; Ovaskainen et al., 2022a, 2022b). Documentation of the topological relationships between lineaments enables, for example, analysis of the abutment relationships between azimuth sets, which could be analysed in a future study to reveal potential age differences between the lineaments (Procter and Sanderson, 2018; Skyttä et al., 2021). Nordbäck et al. (2023) used the current lineament database within a multiscale study on brittle structural frameworks and demonstrated that the lineament data can be applied in detailed site studies in crystalline bedrock settings. Even though specific site characterization studies acquire more detailed site studies and fieldwork for the assessment of crystalline bedrock suitability, this lineament database can be utilized in the first stage of site screening.

The trend maxima of NW–SE-trending lineaments (Figure 10) is evident in the whole country, except for northern Finland, where the lineament orientations are more evenly distributed. This might be attributed to the ice movement direction, which in most parts of Finland was parallel to this lineament set and accordingly enhanced the occurrence of lineaments in that orientation due to scouring of the bedrock during glacial flow (Skyttä et al., 2015; Ovaskainen et al., 2022b). In the rose plots for tectonic provinces, the different areas display similar lineament orientations as seen for the whole country, but the Southern Finland Subprovince display more diverse orientations. This is probably due to the geological characteristics of this tectonic subprovince, where the lineaments reflect prominent geological structures in the bedrock and distinct Quaternary glacially derived formations (Skyttä et al., 2015; Torvela and Kurhila, 2022). The other provinces in Finland are also differently affected by erosional processes (Hall et al., 2021), which is especially evident in western Finland, where a flatter topographical surface especially hinders the identification of topographical lineaments.

The present work has provided a new lineament database for Finland, which is more flexible for statistical analysis and correlation than those that have been available so far. This database will be a part of the public domain of the Geological Survey of Finland (https://hakku.gtk.fi/en/locations/search?location_id=154), and all the trace vector datasets are available for further use. Each lineament trace has a unique identifier (Lineament_ID; Table 1), which can be used to

355   consistently reference each lineament separately in any work using the lineaments, whether in research or in industry. Performing a structural lineament interpretation is an important component of the assessment of a crystalline bedrock setting, where the interpreted lineaments have the potential to represent the surface expression of faults and fractures that may act as potential groundwater flow pathways, zones of geomechanical instability or potential reactivation. The current lineament database will be applied as a basis for various more detailed studies, such as groundwater site studies,

360   infrastructure studies for tunnels, highways and railroads, but also in geological bedrock and tectonic studies.

Conclusions

- This nationwide lineament interpretation of Finland used magnetic raster maps, electromagnetic raster maps and a LiDAR DEM together with bathymetric data to produce three new separate lineament vector datasets.
- An integrated lineament vector dataset was produced through the compilation of all three above-mentioned

365   datasets.
- The interpretation of lineaments preserves the abutments between lineaments and thus adds key insights into the topological relationships between lineaments.
- The lineament vector datasets can be used in further interpretations and scales where they can be compared with more detailed lineament interpretation and other datasets.

370   - However, the lineaments must be verified and examined to determine the true geological nature of the features.
- These lineament vector datasets are publicly available from the Geological Survey of Finland and can be exploited in a wide variety of geological studies.

Credit authorship contribution statement:

Jon Engström: Conceptualization, Methodology, Interpretation, Visualization, Writing - original draft **Mira**

375   **Markovaara-Koivisto**: Conceptualization, Interpretation, Visualization, Writing - review & editing. **Nikolas Ovaskainen**: Conceptualization, Validation, Visualization, Writing - review & editing. **Nicklas Nordbäck:** Conceptualization, Writing - review & editing. **Markku Paananen:** Conceptualization, Review. **Ismo Aaltonen:** Interpretation, Review. **Annu Martinkauppi:** Interpretation, Review. **Heidi Laxström:** Interpretation, Review. **Henrik Wik**: Interpretation, Review.

380   **Acknowledgements**

This study was funded by the project Kallioperän rikkonaisuus – Bedrock fracturing (50402-20101) at the Geological Survey of Finland. The authors also wish to give a special thanks to K. Nikkilä for constructive comments on an early version of the manuscript.

385

390

395

Appendix A: Magnetic total field DGRF-65 greyscale anomaly raster map (Geological Survey of Finland, 2007a).
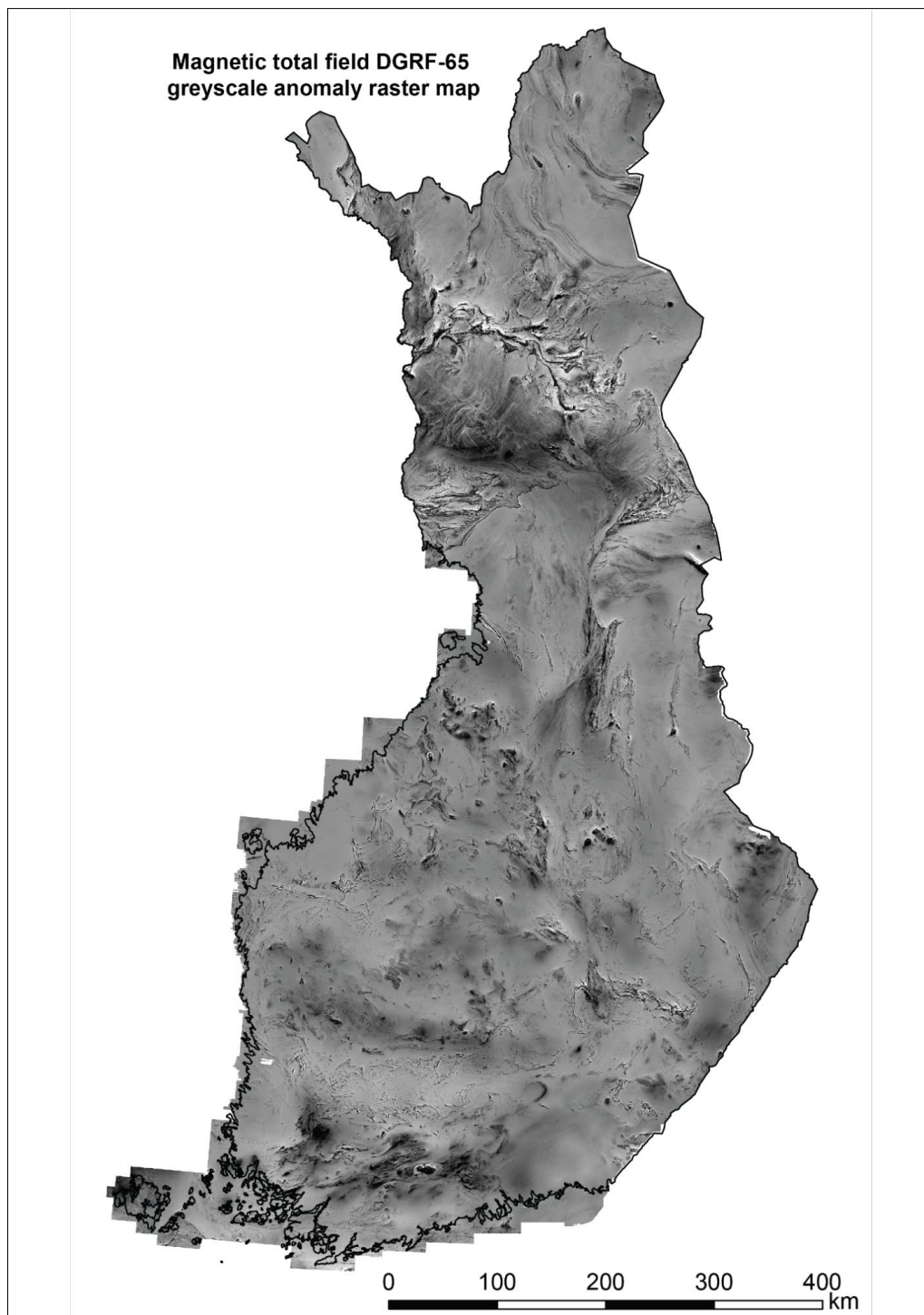
Appendix B: Magnetic sharp-filtered total field DGRF-65 greyscale anomaly raster map (Geological Survey of Finland, 2007a).
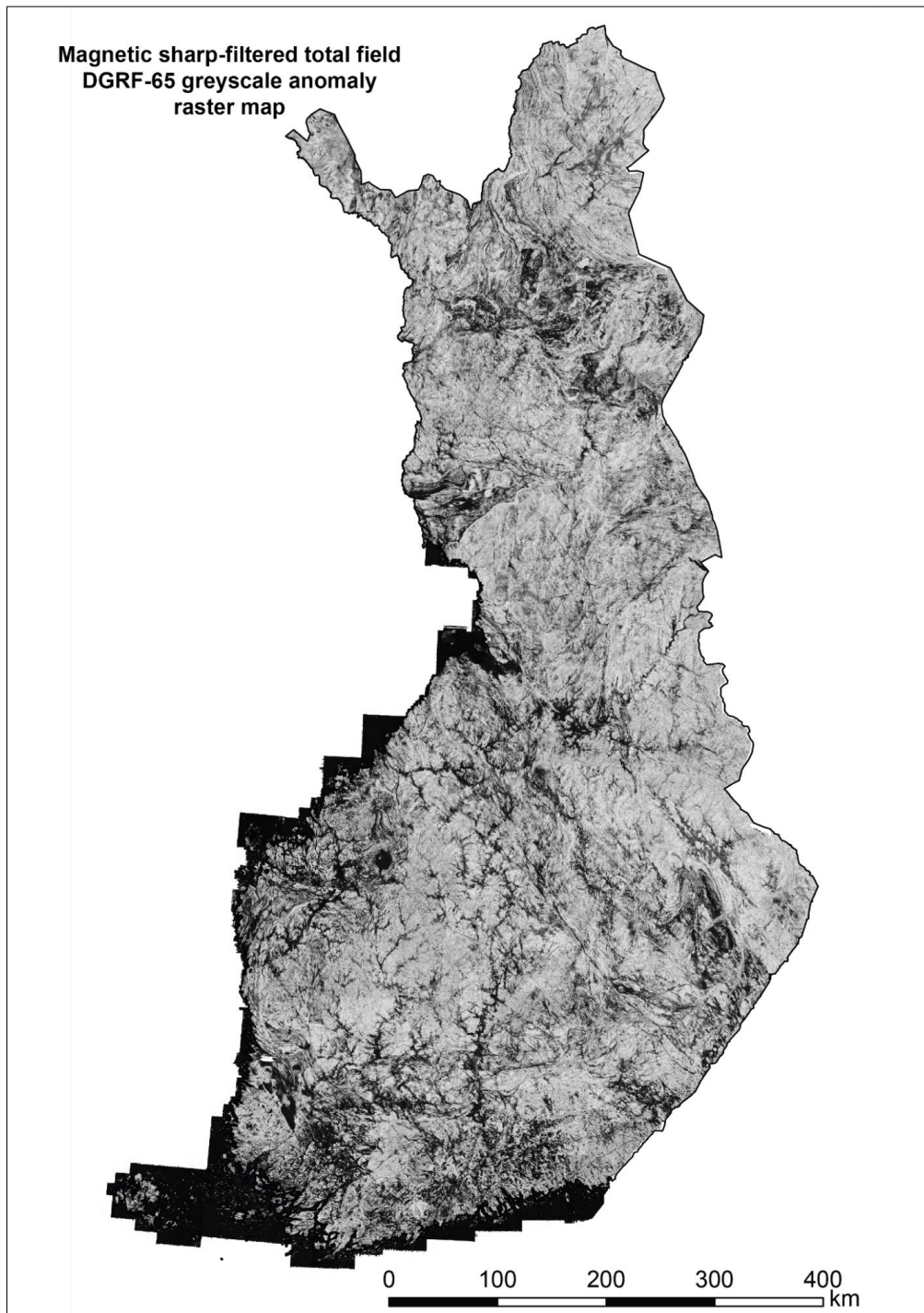
Appendix C: Magnetic anomaly tilt derivate DGRF-65 greyscale raster map (Geological Survey of Finland, 2007a).

405   **Appendix D:** Electromagnetic 3kHz quadrature component greycale raster map (Geological Survey of Finland, 2007b).
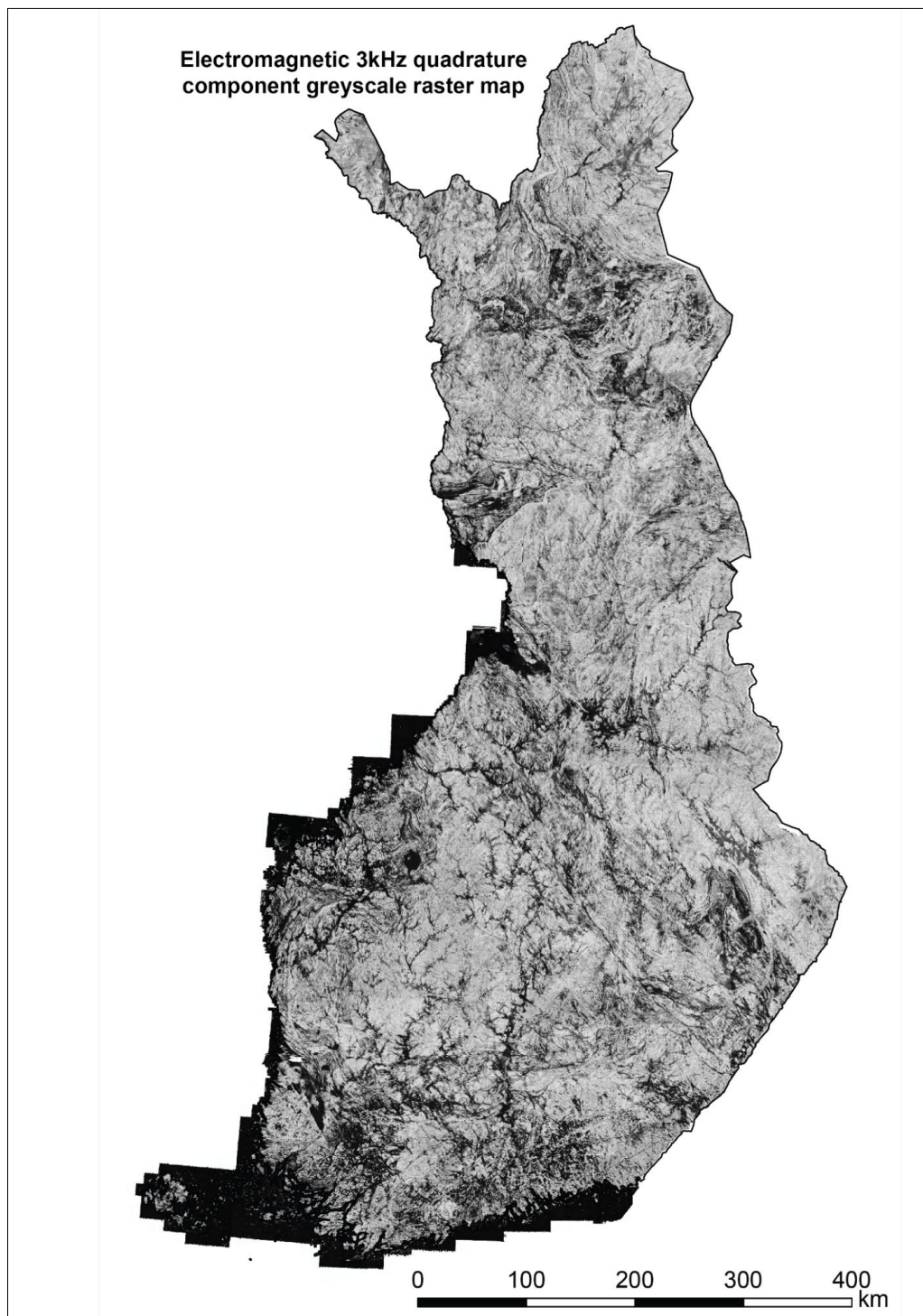
Appendix E: LiDAR and bathymetry multidirectional hillshade DEM. Topographic DEM adapted from (National Land Survey of Finland, 2019) and European EMODnet Bathymetry Consortium (2018).
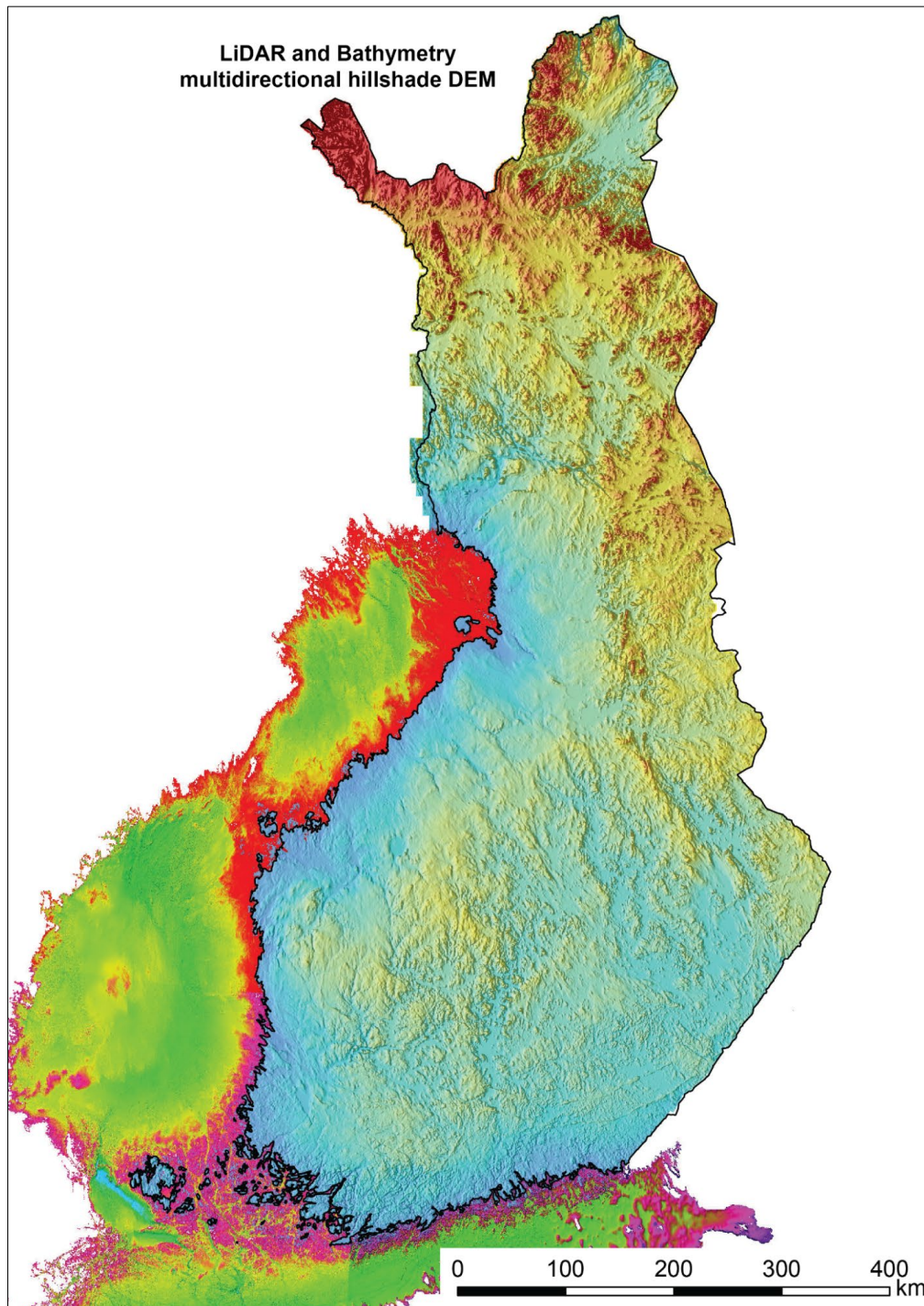
410   **References**

Abdullah, A., Nassr, S., Ghaleeb, A., 2013. Remote Sensing and Geographic Information System for Fault
        Segments Mapping a Study from Taiz Area, Yemen. Journal of Geological Research 2013, e201757.
        https://doi.org/10.1155/2013/201757

Abrams, M., Blusson, A., Carrere, V., Nguyen, T., Rabu, Y., 1985. Image processing applications for geologic
415   mapping. IBM Journal of Research and Development 29, 177–187.
        https://doi.org/10.1147/rd.292.0177

Aghaee, A., Shamsipour, P., Hood, S., Haugaard, R., 2021. A convolutional neural network for semi-
        automated lineament detection and vectorisation of remote sensing data using probabilistic
        clustering: A method and a challenge. Computers & Geosciences 151, 104724.
420   https://doi.org/10.1016/j.cageo.2021.104724

Ahmadi, H., Pekkan, E., 2021. Fault-Based Geological Lineaments Extraction Using Remote Sensing and
        GIS—A Review. Geosciences 11, 183. https://doi.org/10.3390/geosciences11050183

Bantilan, N., 2020. pandera: Statistical Data Validation of Pandas Dataframes.

Berkowitz, B., 2002. Characterizing flow and transport in fractured geological media: A review. Advances in
425   Water Resources 25, 861–884. https://doi.org/10.1016/S0309-1708(02)00042-8

Bond, C.E., Gibbs, D., Shipton, Z.K., 2007. What do you think this is? " Conceptual uncertainty " in
        geoscience interpretation. Gsa Today 17. https://doi.org/10.1130/GSAT01711A.1

Ceccato, A., Tartaglia, G., Antonellini, M., Viola, G., 2022. Multiscale lineament analysis and permeability
        heterogeneity of fractured crystalline basement blocks. Solid Earth 13, 1431–1453.
430   https://doi.org/10.5194/se-13-1431-2022

DesRoches, A., Sykes, M., Parmenter, A., Sykes, E., 2018. Lineament Interpretation of the Revell Batholith
        and Surrounding Greenstone Belts. NWMO Report No. NWMO-TR-2018-19. Nuclear Waste
        Management Organization, Toronto.

EMODnet Bathymetry Consortium, 2018. EMODnet Digital Bathymetry (DTM 2018). [WWW Document],
435   EMODnet Bathymetry Consortium. URL http://doi.org/10.12770/18ff0d48-b203-4a65-94a9-
        5fd8b0ec35f6

Engström, J., Klint, K., 2014. Continental Collision Structures and Post-Orogenic Geological History of the
        Kangerlussuaq Area in the Southern Part of the Nagssugtoqidian Orogen, Central West Greenland.
        Geosciences 4, 316–334. https://doi.org/10.3390/geosciences4040316

440 Gabrielsen, R., Braathen, A., Dehls, J., Roberts, D., 2002. Tectonic lineaments of Norway. Norsk Geologisk
        Tidsskrift 82.

Geiger, S., Emmanuel, S., 2010. Non-Fourier thermal transport in fractured geological media: NON-FOURIER
        THERMAL TRANSPORT. Water Resources Research 46. https://doi.org/10.1029/2009WR008671

Geological Survey of Finland, 2007a. Aeromagnetic raster data of Finland., Hakku, Geological Survey of
445   Finland. https://hakku.gtk.fi/en/locations/search

Geological Survey of Finland, 2007b. Aeroelectromagnetic raster data of Finland., Hakku, Geological Survey
        of Finland. https://hakku.gtk.fi/en/locations/search

Hall, A.M., Putkinen, N., Hietala, S., Lindsberg, E., Holma, M., 2021. Ultra-slow cratonic denudation in
        Finland since 1.5 Ga indicated by tiered unconformities and impact structures. Precambrian
450   Research 352, 106000. https://doi.org/10.1016/j.precamres.2020.106000

Hautaniemi, H., Kurimo, M., Multala, J., Leväniemi, H., Hautaniemi, J., 2005. The" Three In One"
        aerogeophysical concept of GTK in 2004. Special Paper - Geological Survey of Finland 39, 21–74.

Henderson, P.J., 1988. Sedimentation in an esker system influenced by bedrock topography near Kingston,
        Ontario. Canadian Journal of Earth Sciences 25, 987–999. https://doi.org/10.1139/e88-098

455 Hobbs, W.H., 1911. Repeating patterns in the relief and in the structure of land. GSA Bulletin 22, 123–176.
        https://doi.org/10.1130/GSAB-22-123

Hobbs, W.H., 1904. Lineaments of the Atlantic Border region. GSA Bulletin 15, 483–506.
        https://doi.org/10.1130/GSAB-15-483

Jennes, J., 2013. DEM surface tools. Jenness enterprises. [WWW Document]. URL http://
460   www.jennessent.com/arcgis/surface_area.htm.

Korhonen, K., Kuivamäki, A., Paananen, M., Paulamäki, S., 2005. Lineament Interpretation of the Olkiluoto Area. Working Report No. 2005–34, Posiva Working Report. Posiva Oy, Eurajoki.

Krabbendam, M., Bradwell, T., 2014. Quaternary evolution of glaciated gneiss terrains: pre-glacial weathering vs. glacial erosion. Quaternary Science Reviews 95, 20–42. https://doi.org/10.1016/j.quascirev.2014.03.013

Kuivamäki, A., 2000. Lineament database of the Finnish potential repository sites for the calculation of bedrock movements induced by earthquakes. No. 2000–12, Posiva Working Report.

Ledésert, B., Dubois, J., Genter, A., Meunier, A., 1993. Fractal analysis of fractures applied to Soultz-sous-Forets hot dry rock geothermal program. Journal of Volcanology and Geothermal Research 57, 1–17. https://doi.org/10.1016/0377-0273(93)90028-P

Manzocchi, T., 2002. The connectivity of two-dimensional networks of spatially correlated fractures. Water Resources Research 38, 1-1-1–20. https://doi.org/10.1029/2000WR000180

Middleton, M., Schnur, T., Sorjonen-Ward, P., 2015. Geological lineament interpretation using the object-based image analysis approach: Results of semi-automated analyses versus visual interpretation. Geological Survey of Finland, Special Paper 57 2015, 20.

Munier, R., 2004. Statistical analysis of fracture data, adapted for modelling Discrete Fracture Networks Version 2. Technical Report. Svensk Kärnbränslehantering AB, Stockholm.

National Land Survey of Finland, 2019. Laser scanning 2008-2019 by National Land Survey of Finland., National Land Survey of Finland. https://www.maanmittauslaitos.fi/en/maps-and-spatial-data/expert-users/product-descriptions/laser-scanning-data

Nironen, M., 2017. Bedrock of Finland at the scale 1:1 000 000 – Major stratigraphic units, metamorphism and tectonic evolution, Geological Survey of Finland, Special Paper 60.

Nordbäck, N., Ovaskainen, N., Markovaara-Koivisto, M., Skyttä, P., Ojala, A., Engström, J., Nixon, C., 2023. Multiscale mapping and scaling analysis of the censored brittle structural framework within the crystalline bedrock of southern Finland. Bulletin of the Geological Society of Finland 95 (1).

Ovaskainen, N., 2022. Tracerepo. Zenodo. https://doi.org/10.5281/zenodo.5930283

Ovaskainen, N., Nordbäck, N., Skyttä, P., Engström, J., 2022a. A new subsampling methodology to optimize the characterization of two-dimensional bedrock fracture networks. Journal of Structural Geology 155, 104528. https://doi.org/10.1016/j.jsg.2022.104528

Ovaskainen, N., Skyttä, P., Nordbäck, N., Engström, J., 2022b. Detailed investigation of multi-scale fracture networks in glacially abraded crystalline bedrock at Åland Islands, Finland. Solid Earth. https://doi.org/10.5194/egusphere-2022-1363

Paananen, M., 2013. Completed Lineament Interpretation of the Olkiluoto Region. Posiva Report No. 2013–02. Posiva Oy, Eurajoki.

Palmu, J.-P., Ojala, A.E., Ruskeeniemi, T., Sutinen, R., Mattila, J., 2015. LiDAR DEM detection and classification of postglacial faults and seismically-induced landforms in Finland: a paleoseismic database. GFF 137, 344–352.

Prabhakaran, R., Bruna, P.-O., Bertotti, G., Smeulders, D., 2019. An automated fracture trace detection technique using the complex shearlet transform. Solid Earth 10, 2137–2166. https://doi.org/10.5194/se-10-2137-2019

Procter, A., Sanderson, D.J., 2018. Spatial and layer-controlled variability in fracture networks. Journal of Structural Geology, Spatial Arrangement of Fractures and Faults 108, 52–65. https://doi.org/10.1016/j.jsg.2017.07.008

Ramli, M.F., Yusof, N., Yusoff, M.K., Juahir, H., Shafri, H.Z.M., 2010. Lineament mapping and its application in landslide hazard assessment: a review. Bulletin of Engineering Geology and the Environment 69, 215–233. https://doi.org/10.1007/s10064-009-0255-5

Reimers, S., Engström, J., Riller, U., 2018. The Kynsikangas shear zone, Southwest Finland: Importance for understanding deformation kinematics and rheology of lower crustal shear zones. Lithosphere 2018 - Tenth Symposium on the Structure, Composition and Evolution of the Lithosphere in Fennoscandia. Programme and Extended Abstracts. INSTITUTE OF SEISMOLOGY UNIVERSITY OF HELSINKI REPORT S-67.

Rohrbaugh, M.B.Jr., Dunne, W.M., Mauldon, M., 2002. Estimating fracture trace intensity, density, and mean length using circular scan lines and windows. AAPG Bulletin 86, 2089–2104.

Sanderson, D.J., Nixon, C.W., 2015. The use of topology in fracture network characterization. Journal of Structural Geology 72, 55–66. https://doi.org/10.1016/j.jsg.2015.01.005

Sanderson, D.J., Peacock, D.C.P., 2020. Making rose diagrams fit-for-purpose. Earth-Science Reviews 201, 103055. https://doi.org/10.1016/j.earscirev.2019.103055

Scheiber, T., Fredin, O., Viola, G., Jarna, A., Gasser, D., Łapińska-Viola, R., 2015. Manual extraction of bedrock lineaments from high-resolution LiDAR data: methodological bias and human perception. GFF 137, 362–372. https://doi.org/10.1080/11035897.2015.1085434

Skyttä, P., Kinnunen, J., Palmu, J.-P., Korkka-Niemi, K., 2015. Bedrock structures controlling the spatial occurrence and geometry of 1.8Ga younger glacifluvial deposits — Example from First Salpausselkä, southern Finland. Global and Planetary Change 135, 66–82. https://doi.org/10.1016/j.gloplacha.2015.10.007

Skyttä, P., Ovaskainen, N., Nordbäck, N., Engström, J., Mattila, J., 2021. Fault-induced mechanical anisotropy and its effects on fracture patterns in crystalline rocks. Journal of Structural Geology 146, 104304. https://doi.org/10.1016/j.jsg.2021.104304

Soliman, A., Han, L., 2019. Effects of vertical accuracy of digital elevation model (DEM) data on automatic lineaments extraction from shaded DEM. Advances in Space Research 64, 603–622. https://doi.org/10.1016/j.asr.2019.05.009

Tailor, A., Cross, A., Hogg, D.C., Mason, D.C., 1986. Knowledge-based interpretation of remotely sensed images. Image and Vision Computing 4, 67–83. https://doi.org/10.1016/0262-8856(86)90026-0

Tirén, S.A., 1991. Geological setting and deformation history of a low-angle fracture zone at Finnsjön, Sweden. Journal of Hydrology 126, 17–43. https://doi.org/10.1016/0022-1694(91)90199-R

Torvela, T., Kurhila, M., 2022. Timing of syn-orogenic, high-grade transtensional shear zone formation in the West Uusimaa Complex, Finland. Bulletin of the Geological Society of Finland 18. https://doi.org/10.17741/bgsf/94.1.001

Verduzco, B., Fairhead, J.D., Green, C.M., MacKenzie, C., 2004. New insights into magnetic derivatives for structural mapping. The Leading Edge 23, 116–119. https://doi.org/10.1190/1.1651454

Vuorela, P., Äikäs, T., 1984. Site selection studies for final disposal of spent nuclear fuel in Finland. Nuclear Waste Disposal Research Report 39 No. 39. Geological Survey of Finland.

Yeomans, C.M., Middleton, M., Shail, R.K., Grebby, S., Lusty, P.A.J., 2019. Integrated Object-Based Image Analysis for semi-automated geological lineament detection in southwest England. Computers & Geosciences 123, 137–148. https://doi.org/10.1016/j.cageo.2018.11.005

Zeeb, C., Gomez-Rivas, E., Bons, P.D., Blum, P., 2013. Evaluation of sampling methods for fracture network characterization using outcrops. AAPG Bulletin 97, 1545–1566. https://doi.org/10.1306/02131312042